Steinberger, B., Seidel, M.-L., Torsvik, T. (2017): Limited true polar wander as evidence that Earth's nonhydrostatic shape is persistently triaxial. - *Geophysical Research Letters*, *44*, 2, pp. 827—834.

DOI: http://doi.org/10.1002/2016GL071937

AGU PUBLICATIONS

Geophysical Research Letters

RESEARCH LETTER
10.1002/2016GL071937

Key Points:
- For a wide range of models, predicted amounts of true polar wander between 70 and 90 Ma by far exceed observed amounts
- Increased stability of pole after 70 Ma is related to a shift from more subduction in the North and South Pacific toward East and West
- Mismatch before 70 Ma possibly indicates additional slabs in the lowermost mantle below both polar regions stabilizing the rotation axis

Supporting Information:
- Supporting Information S1
- Movie S1
- Movie S2
- Movie S3
- Movie S4
- Movie S5
- Movie S6

Correspondence to:
B. Steinberger,
bstein@gfz-potsdam.de

Citation:
Steinberger, B., M.-L. Seidel, and T. H. Torsvik (2017), Limited true polar wander as evidence that Earth's nonhydrostatic shape is persistently triaxial, *Geophys. Res. Lett.*, *44*, 827–834, doi:10.1002/2016GL071937.

Received 15 NOV 2016
Accepted 9 JAN 2017
Accepted article online 14 JAN 2017
Published online 28 JAN 2017

Limited true polar wander as evidence that Earth's nonhydrostatic shape is persistently triaxial

Bernhard Steinberger[1,2], Miriam-Lisanne Seidel[3], and Trond H. Torsvik[1,2,4,5]

[1]Section 2.5 Geodynamic Modelling, GFZ German Research Centre for Geosciences, Potsdam, Germany, [2]Centre for Earth Evolution and Dynamics, University of Oslo, Oslo, Norway, [3]Werner-von-Siemens Gymnasium, Berlin, Germany, [4]Geological Survey of Norway (NGU), Trondheim, Norway, [5]School of Geosciences, University of Witwatersrand, Wits, South Africa

Abstract Earth's spin axis follows the maximum moment of inertia axis of mantle convection, with some delay due to adjustment of the rotational bulge. Here we compute this axis for geodynamic models based on subduction history, assuming constant slab sinking speed, with another contribution due to thermochemical piles. For a wide range of parameters, a large shift of ≈90° is predicted around 80–90 Ma. It can be largely attributed to a change in circum-Pacific subduction from predominantly in the North and South toward East and West. Actual amounts of true polar wander are much smaller, pointing toward additional inertia tensor contributions, possibly due to slabs in the lowermost mantle below both polar regions. These slabs would have been subducted before ≈150 Ma, when plate motions in the Panthalassa basin are largely unknown. Matching predicted and observed true polar wander can serve at constraining such plate motions.

1. Introduction

When the Earth's mantle and lithosphere, as a whole, change their orientation relative to the rotation axis, it could also be viewed, in the mantle reference frame, as motions of the rotation pole. Hence, this process is termed "true polar wander" (TPW) (see *Courtillot* [2007], for a review). On geologic timescales, it is generally believed to mainly result from changes of the mass distribution in Earth's mantle. Accordingly, it can be computed from mantle convection models and therefore possibly serve to constrain such models: If predicted TPW significantly disagrees with observations, some feature(s) of the model must be wrong, and one can therefore aim at modifying the models to achieve better agreement. In this way, considering TPW may lead to an improved understanding of processes in the Earth interior.

Paleomagnetic poles from a given plate will fall along an apparent polar wander path which can be converted to "observed" TPW by correcting for plate motions in a suitable mantle reference frame. For the past ≈130 Myr, a hot spot reference frame can be used. The motion of hot spots—of the order 1 cm/yr, much slower than typical plate motions—can also be estimated and taken into account [*O'Neill et al.*, 2005; *Doubrovine et al.*, 2012].

The pole follows the maximum moment of inertia axis of mantle convection (abbreviated here as MaxMI axis), but lags behind, because the equatorial bulge needs to adjust to changes in the spin axis [*Gold*, 1955; *Cambiotti et al.*, 2011]. With realistic assumptions, one can estimate that the spin axis may move as much as ≈1–2°/Myr [*Steinberger and O'Connell*, 1997; *Tsai and Stevenson*, 2007; *Steinberger and Torsvik*, 2010]. If the MaxMI axis moves much slower than this and is already close to the spin axis, they both will remain closely aligned. This has probably been the case during the Cenozoic [*Steinberger and O'Connell*, 1997; *Steinberger and Torsvik*, 2010].

Past mantle density can be inferred from seismic tomography through backward advection [*Steinberger and O'Connell*, 1997] or the adjoint method [*Bunge et al.*, 2003], but the fraction of mantle density anomalies that cannot be reliably reconstructed gets larger and larger further back in time. Therefore, to model TPW during the Mesozoic or even Paleozoic, an alternative forward modeling approach, where mantle density through time is based on subduction history and the sinking of slabs [*Richards et al.*, 1997], becomes more attractive. The drawback is that this approach essentially only considers the downward limb of convection. In a limited way, one can consider the effect of upwellings by assigning an inertia tensor contribution to the Large Low

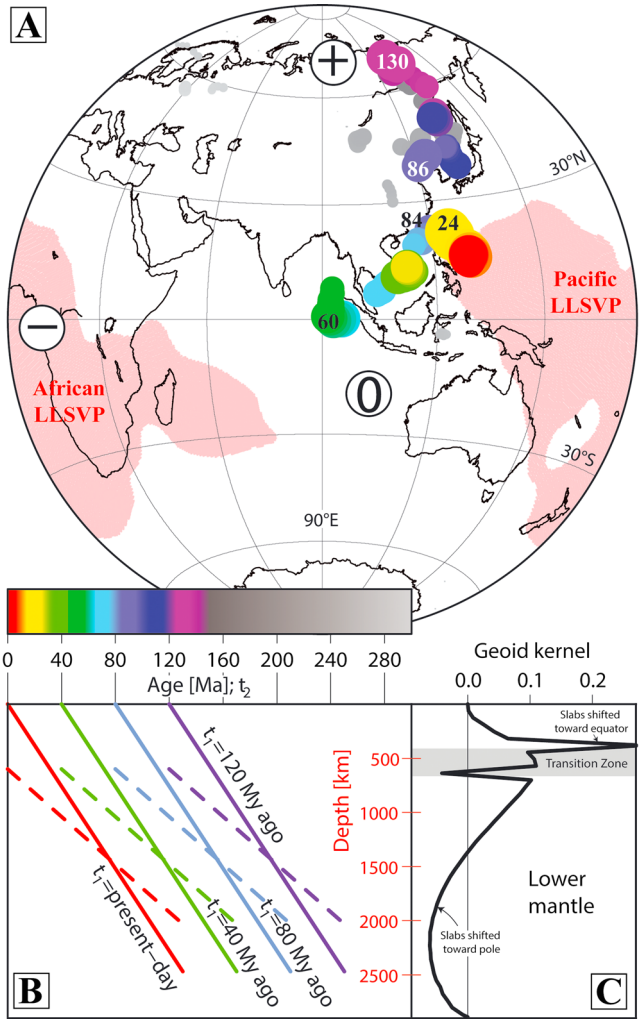

Figure 1. (a) Calculated minimum moment of inertia (MoI) axis of (uncompensated) slabs versus subduction age, indicated by color. Size of circles corresponds to difference between intermediate and minimum MoI. LLSVPs (Large Low Shear-wave Velocity Provinces) indicated in pink, with symbols plus, minus, and zero for their axis of maximum, minimum, and intermediate MoI. (b) Depth of subducted slabs versus slab age t_2 for different times t_1 (corresponding to line color) before present. Curves change as slabs sink through the mantle. Continuous lines for equation (1), dashed lines for equation (2). (c) Degree 2 geoid kernel [*Steinberger and Calderwood*, 2006] as weighting factor of how much slabs at given depth contribute to the total MoI tensor.

Shear Velocity Provinces (LLSVPs) under Africa and the Pacific (Figure 1a), where probably most of the upwelling flow occurs [*Rouby et al.*, 2010; *Steinberger and Torsvik*, 2010]. Since the LLSVPs correspond to geoid highs, they are assigned an inertia tensor contribution with the axis of minimum moment of inertia (MoI) near their centers, and intermediate and maximum axes ≈90° away (Figure 1a). Because the difference between maximum and intermediate MoI of the LLSVPs is much smaller than the difference between their intermediate and minimum MoI, the total MaxMI axis tends to stay near a great circle halfway between the two LLSVPs, and the distribution of slabs determines where, approximately along this circle, the MaxMI axis occurs. However, upwellings above LLSVPs and their margins could be quite time-dependent, even if the LLSVPs themselves are not, and any changes in the inertia tensor due to this time dependence cannot be modeled reliably.

Rouby et al. [2010] and *Steinberger and Torsvik* [2010] predict rather large amounts of TPW over the past 120–130 Myr, much exceeding observations. In *Steinberger and Torsvik* [2010] large motions only occur before 100 Ma. Limited TPW after 100 Ma was also emphasized by *Richards et al.* [1997], but even they find fast TPW (see their Figure 3) before 100 Ma. In contrast, paleomagnetic reconstructions indicate much less observed TPW back to 320 Ma [*Steinberger and Torsvik*, 2008]. Here we aim at better understanding this discrepancy and pointing at possible ways to resolve it. Whereas *Steinberger and Torsvik* [2010] used a dynamic mantle flow model based on subduction history, here we adopt the simpler approach of assuming vertical slab sinking with prescribed speed [*Richards et al.*, 1997; *Rouby et al.*, 2010]. In this way, we can run a much larger number of models and test how results depend on various assumptions, and which results are robust. Moreover, a recent comparison of subduction history with seismic topography at various depths in the mantle indicates that a sinking speed that is constant or only depends on depth could be quite an appropriate assumption [*Domeier et al.*, 2016]. We can therefore assign sinking speeds consistent with observations, rather than using those generated within the numerical model.

We will describe our method of computing the MaxMI axis and TPW in the next section. The results section will show a large predicted motion of the MaxMI axis, and hence a large TPW prediction for a wide variety of models. We will then discuss the reasons for this result, which is clearly discrepant with observations and possible ways it could be resolved.

2. Method

Our workflow consists of the following steps:

1. Computing the inertia tensor of (uncompensated) subducted slabs at given times: From plate reconstructions, convergence rate is computed. Given the length of each subduction zone element, convergence rate, depth-integrated density anomaly (assumed either constant $2.184 \cdot 10^6$ kg/m^2 or depending on age of subducted lithosphere), and time interval (2 Myr), an anomalous mass is assigned to each subduction zone element. Besides the reference case [*Steinberger and Torsvik*, 2010] for 0–300 Ma, we use several other plate reconstructions to account for uncertainties. The minimum MoI axis through time for the reference case is shown in Figure 1a. This corresponds to the regions where most subduction occurs (and/or around its antipode) and the convergent quadrupoles of *Conrad et al.* [2013].
2. Converting age to depth: Following *Domeier et al.* [2016] we assign slabs subducted at a given time t_2 in the past, before the time t_1 for which the inertia tensor is to be computed, to depth z. We vary the age-depth relationship between

$$z\left(t_1, t_2\right) = 1.9 \text{ cm/yr} \cdot \left(t_2 - t_1\right) \tag{1}$$

(reference case) and

$$z\left(t_1, t_2\right) = 1.1 \text{ cm/yr} \cdot \left(t_2 - t_1\right) + 600 \text{ km}. \tag{2}$$

In the first (second) case, slabs take 153 Myr (209 Myr) to sink to the base of the mantle, i.e., 300 Myr of subduction history allows TPW prediction back to 147 (91) Ma. In the latter case, slabs are inserted at depth 600 km. Results remain very similar with a faster slab sinking rate in the upper mantle; hence, we maintain our simpler assumption equation (2).
3. Computing contribution of slabs at given depth to inertia tensor: Subducting slabs induce flow in the mantle and this flow causes dynamic topography at the Earth surface and core mantle boundary (CMB). These topographies also affect the inertia tensor, partly *compensating* or even *overcompensating* the effect of the slab density anomalies. In case of viscosity only varying with radius, this can be expressed in terms of a depth-dependent kernel, which specifies the fraction of the MoI, compared to the one caused by the same *uncompensated* density anomaly pattern at the surface. We assume here that this density anomaly pattern does not change as slabs sink in the mantle. This is not strictly the case, as slabs geometrically widen, relative to the reduced radius at depth, but the effect on the inertia tensor could be more or less compensated (within uncertainties) by reduced thermal expansivity at depth. Since the MoI tensor is related to the degree 2 geoid coefficients according to McCullagh's formula, we use the degree 2 geoid kernel $K_2(z)$. Spikes at 410 and 660 km (top and bottom of the transition zone; Figure 1c) account for phase boundaries, such that the integral over the kernels corresponds to the total phase boundary effect.
4. Computing the total inertia tensor: First, we add the contribution at each time for all slabs above a certain maximum depth z_{max}. The default value (reference case) for z_{max} is at the CMB, but since *Domeier et al.* [2016] find a decorrelation of slabs and tomography in the lowermost mantle, we also consider cases with slabs only included to a smaller z_{max}. This corresponds to assuming that, below that depth, slabs no longer sink vertically but distribute laterally over the CMB. Second, we add a constant "background inertia tensor." In our reference case, we adopt this contribution from *Steinberger and Torsvik* [2010], where it has been estimated assuming it is related to the LLSVPs. However, we also consider other cases described in the results section.
5. Computing the MaxMI axis and (optionally) TPW. Given the shape of the kernels in point (3), this axis tends to be located such that slabs in the upper mantle are far away, but slabs in the lower mantle close by. From the MaxMI axis, TPW can be computed, considering that the spin axis does not instantaneously follow the MaxMI axis, due to adjustment of the equatorial bulge. However, in most cases, for the sake of simplicity, we will not do this final step. This will be further justified in the results section.

3. Results

Figure 2 shows results for the reference case with age-depth relation equation (1) and slabs included to CMB depth. For the present day, the MaxMI axis is <3° from the North Pole. Also, the trend and speed of motion for the last 10 Myr is similar to observed. However, discrepancies become larger further back in time, and the predicted MaxMI axis moves by almost 90° around 80–90 Ma. For the observed TPW of the last 120–130 Myr,

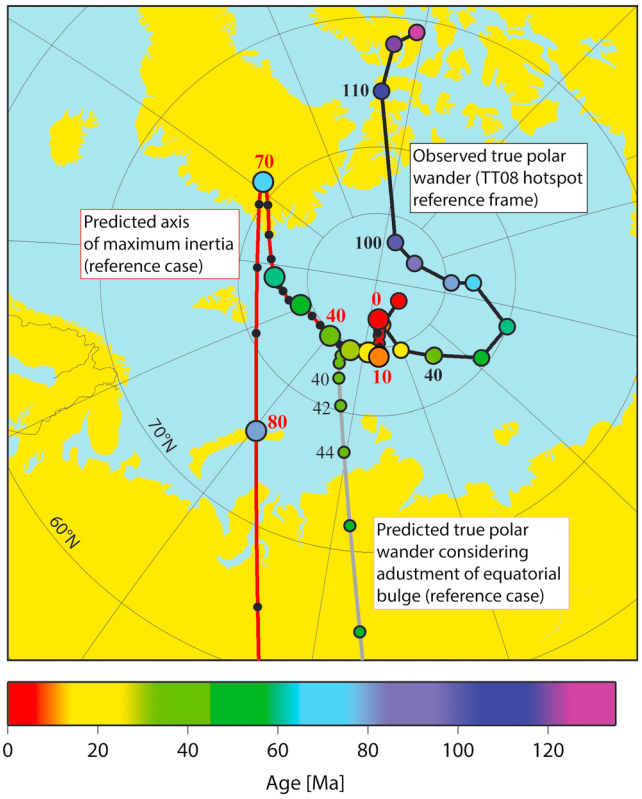

Figure 2. Predicted MaxMI axis (maximum moment of inertia axis of mantle convection) in the reference case (red line). For comparison, we also show predicted TPW (true polar wander), under consideration of its speed limit due to adjustment of the equatorial bulge (grey line), and observed TPW in the global mantle reference frame of *Torsvik et al.* [2008]. Bold numbers indicate ages in Ma.

the largest motion of ≈10° occurs in a similar direction 100–110 Ma. Computation of the spin axis, following the procedure described in *Steinberger and Torsvik* [2010], leads to the TPW curve shown as grey line with small colored circles in 2 Myr intervals: Since the most rapid change of ≈90° of the MaxMI axis occurs around 80–90 Ma, and the maximum speed of TPW is ≈2°/Myr, it is only after 40 Ma that the predicted spin axis comes and stays close to the MaxMI axis. Therefore, this last step rather increases the discrepancies with observed TPW.

If the age-depth relation of slabs is changed to equation (2) (Figure 3a; curve marked "2900 slow"; Movie S1 in the supporting information), corresponding to faster sinking in the upper mantle and slower sinking in the lower mantle, the misfit of the present-day pole is substantially larger, but otherwise results remain similar, especially a fast motion, in a very similar direction, is still predicted between 80 and 90 Ma. Since *Domeier et al.* [2016] show that the correlation of subduction zones with tomography deteriorates below depth 2300 km, we also include a curve (marked "2300 slow"), where only slabs above depth 2300 km are considered. It fits the present-day pole better, but otherwise remains very similar. For faster slab sinking, fast motion of the MaxMI axis would occur at an earlier time, more similar to the model of *Steinberger and Torsvik* [2010] and observed TPW. However, such fast sinking would be inconsistent with *Domeier et al.* [2016]. With only slabs above a certain depth and age-depth relation equation (1) (Figure 3b; curves marked "2300" and "1400"; Movie S2 in the supporting information) results remain similar to the reference case, but poles are shifted toward Greenland after 70 Ma, and fast motion before that is mostly in the opposite direction.

We now turn to varying the LLSVP contribution (Figure 3c; Movie S3 in the supporting information). If the constant MoI tensor assigned to the LLSVPs is reduced (increased), the MaxMI axis is less (more) constrained to remain close to halfway between the LLSVPs, and the motion of the MaxMI axis toward the Pacific LLSVP between ≈70 and 10 Ma varies accordingly. However, we still obtain a fast motion between 80 and 90 Ma similar to the reference case.

In a further attempt to reduce this fast motion, we make the "background" inertia tensor triaxial, by reducing the intermediate MoI (Figure 3d, curve "IMI = 0"; Movie 4 in the supporting information). As expected, this reduces the motion of the MaxMI axis, but it still remains too large, ends later than, and goes in the opposite direction to observed TPW.

Further, we modified the background inertia tensor, such that the total inertia tensor (background + slabs contribution) exactly matches observations (Figure 3d, curve marked "total matched"; Movies S5 and S6 in the supporting information) and the present-day MaxMI axis falls exactly on the pole. Given that the axis of minimum MoI of the Earth is further west than the LLSVP centers, the largest predicted motion of the MaxMI axis occurs in a somewhat different direction in these cases, but remains fast during a similar time interval as in the reference case.

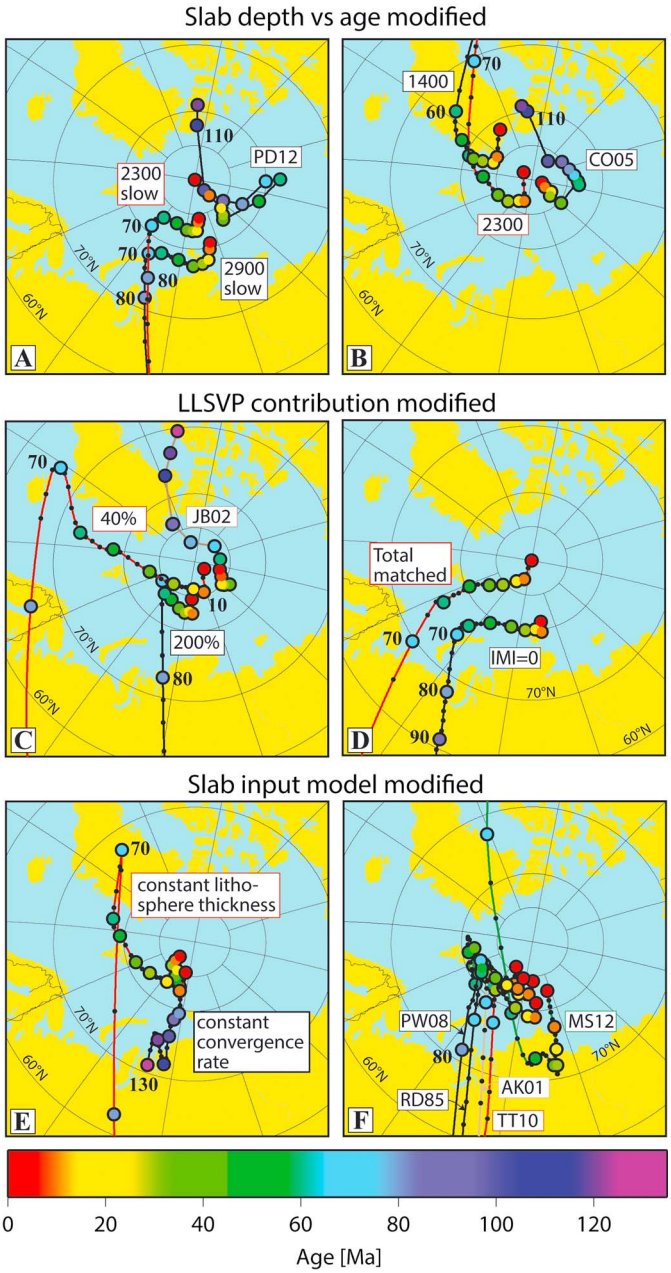

Figure 3. Predicted MaxMI axis for modification cases. Numbers indicate ages in Ma. (a) Sinking of slabs modified to equation (2). Slabs included to CMB (curve marked "2900 slow") or only depth 2300 km (marked "2300 slow," red line). (b) Slabs included to depth 2300 km (marked "2300"; red line) or 1400 km (marked "1400"); otherwise as reference case. (c) LLSVP inertia tensor increased by factor 2 or reduced to 40% (red line), as indicated. (d) Intermediate MoI of "background" reduced to zero (marked "IMI = 0"), or "background" inertia tensor chosen such that total matches observations (marked "total matched"; red line). (e) Results with subduction input as in models 2 and 3 of *Steinberger and Torsvik* [2010], with constant lithosphere thickness (red line) and also constant convergence rate. (f) Subduction input models MS12 [*Seton et al.*, 2012, green line] for 0–200 Ma, TT10 [*Torsvik et al.*, 2010; *Conrad et al.*, 2013, red line] for 0–250 Ma, and three cases RD85, AK01 (light brown line), and PW08 considered by *Conrad et al.* [2013] with different Pacific plate motions [*Duncan and Clague*, 1985; *Koppers et al.*, 2001; *Wessel and Kroenke*, 2008] for 80–150 Ma and 150–250 Ma plate motions as in TT10. Curves in Figure 3f except for MS12, disregard age variations of subducted lithosphere and are very similar. Subduction input before 200 Ma for MS12 and before 250 Ma for other models in Figure 3f as in reference case. Like in Figure 2, predicted TPW follows the predicted MaxMI axis, but with some time delay if the MaxMI axis moves very fast (not shown). For comparison, distributed over Figures 3a–3c for clear visibility, three further cases for "observed" TPW are shown: "PD12" is the African Apparent Polar Wander Path of *Torsvik et al.* [2012] transferred to the global mantle reference frame of *Doubrovine et al.* [2012], "CO05" is in the African mantle reference frame of *O'Neill et al.* [2005], and "JB02" is from *Besse and Courtillot* [2002].

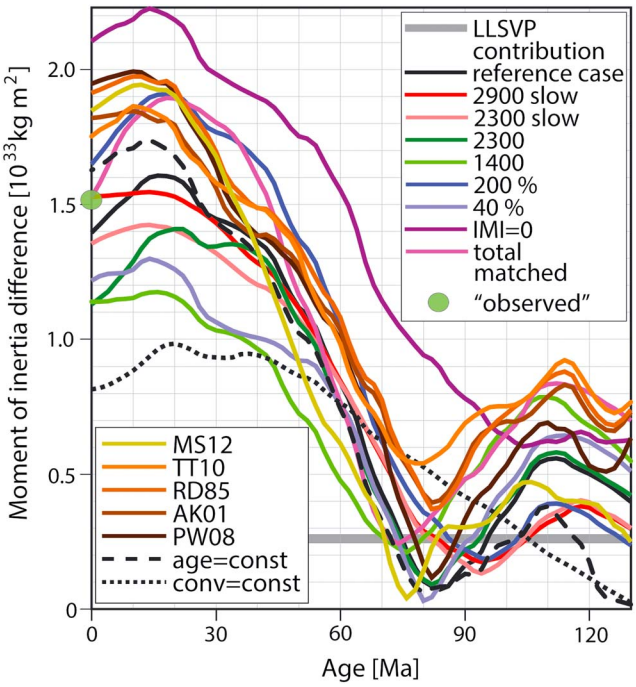

Figure 4. Difference between maximum and intermediate MoI for all cases shown in Figures 2 and 3 as indicated in the legend. Value of LLSVP contribution indicated by thick grey line, for comparison. "age=const", constant lithosphere thickness; "conv=const", constant convergence rate.

In the results obtained so far, we had considered variations in the thickness of subducted slabs, due to different age of subducted lithosphere, back to 140 Ma. The motion of the MaxMI axis remains very similar, if we instead assume a constant lithosphere thickness (red line in Figure 3e). If, however, the convergence rate is also set to be constant for all times, results change considerably, motion of the MaxMI axis is much reduced over the past 130 Myr, but the predicted motion is still rather different from observation-derived TPW, with total motion in approximately the opposite direction.

Results also remain similar for several other plate reconstructions (Figure 3f): The models TT10 and MS12 are based on a plate reconstruction back to 250 Ma (200 Ma), and therefore, in contrast to the results shown so far, also consider variations in convergence rate before 140 Ma. These are rather uncertain, because plate motions in the Pacific hemisphere are very poorly constrained before 140 Ma, but for these models, the predicted MaxMI axis remains very similar. Pacific plate motions are somewhat better constrained between 83 and 140 Ma, and results for three different models remain very similar to TT10.

Further models yielding similar results are not shown: These include changing the longitude of subduction [*van der Meer et al.*, 2010], considering (or disregarding) lithosphere thickness variations with age, neglecting the effects of phase transitions, using different kernels as in *Steinberger and Torsvik* [2010], and using the plate reconstruction of *Matthews et al.* [2016], based on *Müller et al.* [2016] and *Domeier and Torsvik* [2014], and different slab input models for the cases shown in Figures 3a–3d.

4. Discussion

We only consider degree 2 kernels that are negative in the lower part and positive in the upper part of the mantle, similar to Figure 1c. Such a kernel shape is required to explain the long-wavelength geoid based on mantle density anomalies [*Thoraval and Richards*, 1997]. Also, a substantial viscosity increase with depth in the mantle, leading to such a kernel shape, is necessary to obtain realistic speeds of TPW [*Spada et al.*, 1992].

Several of our models predict the present position of the MaxMI axis within a few degrees of the north pole. Whereas the axis for only the LLSVP contribution would be in Northern Siberia, about 19° from the pole, combining this with the subducted slab contribution brings the axis much closer to the pole. Also, the recent trend toward Greenland is approximately matched by these models. Back to ≈70 Ma, most model predictions agree with observations at least insofar as polar motion is less than ≈10–15°, and differences could perhaps be due to variations in upwelling flow, given that backward models, which consider variations in both upward and downward flow, tend to yield a better fit [*Steinberger and O'Connell*, 1997]. The period, for which a rather stable rotation axis is predicted, is limited to after ≈40 Ma, if the speed limit of TPW is considered (Figure 1). Before that, most models predict rather large and fast polar motion, which—based on paleomagnetic data—have only been claimed for much earlier times [e.g., *Kirschvink et al.*, 1997; *Mitchell et al.*, 2010].

Large shifts of the MaxMI axis tend to occur during times when the difference between maximum and intermediate MoI is very small (Figure 4), similar to "Inertial Interchange TPW." Increasing MoI difference past

≈70–80 Ma can be attributed to circum-Pacific subduction becoming predominantly E-W around that time (Figure 1a). Because the degree 2 geoid kernel (Figure 1c) is positive in the upper part of the mantle, the axis of minimum MoI due to slabs only is shifted toward near the equator. This means that for the total inertia tensor (with minimum axis remaining near LLSVP centers) the MaxMI axis is stabilized near the pole. In contrast, the kernel (Figure 1c) is negative in the lower part of the mantle. Therefore, for slabs in the lower part of the mantle, the total MaxMI axis should be near the minimum MoI axis of uncompensated slabs (Figure 1 a). For slabs in the entire mantle, it can be either way, depending on which contribution is dominant. Amounts of subduction are increasingly poorly known further back in time, in particular, around the circum-Pacific. Therefore, both the minimum MoI of slabs (Figure 1a) and the relative (and opposing) contributions from upper and lower mantle are poorly constrained, especially for subduction before ≈140 Ma. Given that for the sinking rates assumed here, slabs take ≈153–209 Ma to sink to the lowermost mantle, we can probably only reliably estimate slab distribution for the largest part of the mantle in the very recent past. This probably corresponds to the relatively good match in the present pole location and recent trend, and decreasing fit, with large shift of the MaxMI axis, further back in time. A similar fast motion also occurred in the fully dynamic models of *Steinberger and Torsvik* [2010], but somewhat earlier. Here slab sinking speed is assigned, based on a comparison with tomography, which could be thought of making the model more realistic, but in fact aggravates problems.

The only cases where the MoI difference as a function of time does not pass through a pronounced minimum around 80–90 Ma in Figure 4 and where accordingly the motion of the MaxMI axis is less fast in Figure 3 are for a modified convergence rate, or a more triaxial background inertia tensor. Hence, rates of convergence different from those assumed here for earlier times are probably responsible for the discrepancies found, and slabs that are now accumulated in the lower mantle could make the "background" inertia tensor more triaxial than inferred from LLSVPs only [see also *Chan et al.*, 2011; *Mitchell*, 2014]. An alternative explanation—that persistent triaxiality is due to long-term elastic strength of the lithosphere, has been proposed by *Creveling et al.* [2012]

5. Conclusions

As lithospheric slabs sink through the mantle, they contribute to mantle density anomalies and cause changes of the inertia tensor and rotation axis (TPW). By comparing TPW predictions with observations, one can therefore test subduction history models for plausibility. Here we perform such "tests" for a variety of models, but all models fail in the sense that predicted changes of the MaxMI axis and TPW clearly disagree with observations. However, closer to the present agreement is better than in the more distant past. We therefore regard it as most likely that the disagreement stems from large uncertainties in absolute plate motions in the Pacific basin, in particular, before ≈140 Ma, leading to erroneous models of circum-Pacific subduction input. In particular, results could possibly be improved if models were modified such that more subduction occurred along the northern and southern margins of the Pacific/Panthalassa, compared to the east and west, before ≈140 Ma. Such models would lead to comparatively more slabs in the lower mantle beneath polar regions, thus keeping the rotation axis more stable and closer to its present position for a longer time. While we regard ad hoc modifications of plate reconstructions as unwarranted, we expect that true polar wander models can be used to constrain future plate reconstructions extending to the more distant past, in particular, if there are several alternatives.

Acknowledgments
We thank Kara Matthews and Simon Williams for plate reconstruction data, and the Alexander von Humboldt Foundation for making this collaboration possible. Figures were mostly produced with the Generic Mapping Tools [*Wessel and Smith*, 1998].

References

Besse, J., and V. Courtillot (2002), Apparent and true polar wander and the geometry of the geomagnetic field over the last 200 Myr, *J. Geophys. Res.*, *107*, 2300, doi:10.1029/2000JB000050.

Bunge, H.-P., C. R. Hagelberg, and B. J. Travis (2003), Mantle circulation models with variational data assimilation: Inferring past mantle flow and structure from plate motion histories and seismic tomography, *Geophys. J. Int.*, *152*, 280–301.

Cambiotti, G., Y. Ricard, and R. Sabadini (2011), New insights into mantle convection true polar wander and rotational bulge readjustment, *Earth Planet. Sci. Lett.*, *310*, 538–543.

Chan, N.-H., J. X. Mitrovica, I. Matsuyama, K. Latychev, J. R. Creveling, S. Stanley, and E. Morrow (2011), The rotational stability of a convecting Earth: The Earth's figure and TPW over the last 100 Myr, *Geophys. J. Int.*, *187*, 773–782.

Conrad, C. P., B. Steinberger, and T. H. Torsvik (2013), Stability of active mantle upwelling revealed by net characteristics of plate tectonics, *Nature*, *498*, 479–482.

Courtillot, V. (2007), True polar wander, in *Encyclopedia of Geomagnetism and Paleomagnetism*, edited by D. Gubbins and E. Herrero-Bervera, pp. 956–969, Springer, Dordrecht, Netherlands, doi:10.1007/978-1-4020-4423-6_308.

Creveling, J. R., J. X. Mitrovica, N.-H. Chan, K. Latychev, and I. Matsuyama (2012), Mechanisms for oscillatory true polar wander, *Nature*, *491*, 244–248.

Domeier, M., and T. H. Torsvik (2014), Plate tectonics in the late Paleozoic, *Geosci. Front.*, *5*, 303–350.

Domeier, M., P. V. Doubrovine, T. H. Torsvik, W. Spakman, and A. L. Bull (2016), Global correlation of lower mantle structure and past subduction, *Geophys. Res. Lett.*, *43*, 4945–4953, doi:10.1002/2016GL068827.

Doubrovine, P. V., B. Steinberger, and T. H. Torsvik (2012), Absolute plate motions in a reference frame defined by moving hot spots in the Pacific, Atlantic, and Indian Oceans, *J. Geophys. Res.*, *117*, B09101, doi:10.1029/2011JB009072.

Duncan, R. A., and D. A. Clague (1985), Pacific plate motion recorded by linear volcanic chains, in *The Pacific Ocean, the Ocean Basins and Margins*, vol. 7A, edited by A. E. M. Nairn, F. G. Stehli, and S. Uyeda, pp. 89–121, Plenum, New York, doi:10.1007/978-1-4613-2351-8_3.

Gold, T. (1955), Instability of the Earth's axis of rotation, *Nature*, *175*, 526–529.

Kirschvink, J. L., R. L. Ripperdan, and D. A. Evans (1997), Evidence for a large-scale reorganization of Early Cambrian continental masses by inertial interchange true polar wander, *Science*, *277*, 541–545.

Koppers, A. A. P., J. P. Morgan, J. W. Morgan, and H. Staudigel (2001), Testing the fixed hot spot hypothesis using $^{40}Ar/^{39}Ar$ age progressions along seamount trails, *Earth Planet. Sci. Lett.*, *185*, 237–252, doi:10.1016/S0012-821X(00)00387-3.

Matthews, K. J., K. T. Maloney, S. Zahirovic, S. E. Williams, M. Seton, and R. D. Müller (2016), Global plate boundary evolution and kinematics since the late Paleozoic, *Global Planet. Change*, *146*, 226–250, doi:10.1016/j.gloplacha.2016.10.002.

Mitchell, R. N. (2014), True polar wander and supercontinent cycles: Implications for lithospheric elasticity and the triaxial Earth, *Am. J. Sci.*, *314*, 966–979, doi:10.2475/05.2014.04.

Mitchell, R. N., D. A. D. Evans, and T. M. Kilian (2010), Rapid Early Cambrian rotation of Gondwana, *Geology*, *38*, 755–758.

Müller, R. D., M. Seton, S. Zahirovic, S. E. Williams, K. J. Matthews, N. M. Wright, G. E. Shephard, K. Maloney, N. Barnett-Moore, and M. Hosseinpour (2016), Ocean basin evolution and global-scale plate reorganization events since Pangea breakup, *Annu. Rev. Earth Pl. Sc.*, *44*, 107–138.

O'Neill, C., D. Müller, and B. Steinberger (2005), On the uncertainties in hot spot reconstructions and the significance of moving hot spot reference frames, *Geochem. Geophys. Geosys.*, *6*, Q0400, doi:10.1029/2004GC000784.

Richards, M. A., Y. Ricard, C. Lithgow-Bertelloni, G. Spada, and R. Sabadini (1997), An explanation for Earth's long-term rotational stability, *Science*, *275*, 372–375.

Rouby, H., M. Greff-Lefftz, and J. Besse (2010), Mantle dynamics, geoid, inertia and TPW since 120 Myr, *Earth Planet. Sci. Lett.*, *292*, 301–311.

Seton, M., et al. (2012), Global continental and ocean basin reconstructions since 200 Ma, *Earth Sci. Rev.*, *113*, 212–270, doi:10.1016/j.earscirev.2012.03.002.

Spada, G., Y. Ricard, and R. Sabadini (1992), Excitation of true polar wander by subduction, *Nature*, *360*, 452–454, doi:10.1038/360452a0.

Steinberger, B., and A. Calderwood (2006), Models of large-scale viscous flow in the Earth's mantle with constraints from mineral physics and surface observations, *Geophys. J. Int.*, *167*, 1461–1481.

Steinberger, B., and R. J. O'Connell (1997), Changes of the Earth's rotation axis owing to advection of mantle density heterogeneities, *Nature*, *387*, 169–173.

Steinberger, B., and T. H. Torsvik (2008), Absolute plate motions and true polar wander in the absence of hotspot tracks, *Nature*, *452*, 620–623.

Steinberger, B., and T. H. Torsvik (2010), Toward an explanation for the present and past locations of the poles, *Geochem. Geophys. Geosys.*, *11*, Q06W06, doi:10.1029/2009GC002889.

Thoraval, C., and M. A. Richards (1997), The geoid constraint in global geodynamics: Viscosity structure, mantle heterogeneity models and boundary conditions, *Geophys. J. Int.*, *131*, 1–8, doi:10.1111/j.1365-246x.1997.tb00591.x.

Torsvik, T. H., R. D. Müller, R. van der Voo, B. Steinberger, and C. Gaina (2008), Global plate motion frames: Toward a unified model, *Rev. Geophys.*, *46*, RG3004, doi:10.1029/2007RG000227.

Torsvik, T. H., B. Steinberger, M. Gurnis, and C. Gaina (2010), Plate tectonics and net lithosphere rotation over the past 150 My, *Earth Planet. Sci. Lett.*, *291*, 106–112, doi:10.1016/j.epsl.2009.12.055.

Torsvik, T. H., et al. (2012), Phanerozoic polar wander, palaeogeography and dynamics, *Earth Sci. Rev.*, *114*, 325–368, doi:10.1016/j.earscirev.2012.06.007.

Tsai, V. C., and D. J. Stevenson (2007), Theoretical constraints on true polar wander, *J. Geophys. Res.*, *112*, B05415, doi:10.1029/2005JB003923.

van der Meer, D. G., W. Spakman, D. J. J. van Hinsbergen, M. L. Amaru, and T. H. Torsvik (2010), Towards absolute plate motions constrained by lower-mantle slab remnants, *Nat. Geosci.*, *3*, 36–40, doi:10.1038/ngeo708.

Wessel, P., and L. Kroenke (2008), Pacific absolute plate motion since 145 Ma: An assessment of the fixed hot spot hypothesis, *J. Geophys. Res.*, *113*, B06101, doi:10.1029/2007JB005499.

Wessel, P., and W. H. F. Smith (1998), New, improved version of generic mapping tools released, *Eos Trans. AGU*, *79*(47), 579–579, doi:10.1029/98EO00426.